scientific reports

Check for updates

OPEN

Loss of fatty acid-binding protein 7 promotes B16F10 melanoma metastasis

Tunyanat Wannakul[1,2], Hirofumi Miyazaki[1]✉, Motoko Maekawa[1], Yoshiteru Kagawa[1], Yui Yamamoto[1,3] & Yuji Owada[1]

Melanoma possesses the characteristic phenotypic plasticity, enhancing its metastatic formation and drug resistance. Lipid and fatty acid metabolism are usually altered to support melanoma progression and can be targeted for therapeutic development. Fatty acid binding protein 7 (FABP7) is highly expressed in melanomas and is shown to support its proliferation, migration, and invasion, but the mechanisms remain unclear. Our study aimed to link FABP7 to lipid metabolism and phenotypic shift in melanomas. We established the *Fabp7*-knockout (KO) B16F10 melanoma cells, which showed an enhanced invasion through matrix-coated membrane, without significant change in proliferation. Similar outcomes were obtained when using RNA interference targeting FABP7. *Fabp7*-KO cells injected into mice exhibited slower primary tumor growth, but formed higher metastatic foci count in the lungs. We also discovered a higher saturation in overall lipids, phosphatidylcholines, and triacylglycerols. We observed transcriptional shifts toward the invasive MITF^{Low}/AXL^{High} phenotype, with upregulation of transforming growth factor-beta (TGF-β) receptor mRNAs. In conclusion, FABP7 may help balancing lipid saturation and maintain the proliferative state of melanomas, mitigating invasiveness and metastatic formation.

Keywords Melanoma, Fatty acid-binding protein 7, Adaptation, Physiological, Neoplasm metastasis, Lipid metabolism

Melanoma is a highly aggressive skin cancer, characterized by its metastatic potential, immune response evasiveness, and resistance to current therapies[1]. Arisen from melanocytes, descendants of embryonic neural crest cells, melanomas acquire the phenotypic plasticity by potentially hijacking their embryonic genetic program[2], allowing them to reversibly shift into various states in response to environmental cues under regulation of several transcription factors, similar to epithelial-to-mesenchymal transition (EMT) found in many epithelial tumor cells[3–8].

Among many candidates, the microphthalmia-associated transcription factor (MITF), and the tyrosine kinase receptor AXL are widely used to mark different states of melanomas[9]. MITF regulates multiple genes accounting for melanoma differentiation antigens, including TYRP1 and MLANA, which involve in melanin production, melanocyte differentiation and proliferation[10,11]. AXL is associated with aggressiveness and drug resistance by signaling through PI3K/AKT, MAPK/ERK and STAT3 pathways[12]. Melanomas with MITF^{High}/AXL^{Low} profile are often linked to the more differentiated and proliferative phenotypes, while MITF^{Low}/AXL^{High} melanomas are more mesenchymal-like, that is, de-differentiated, slow cycling but highly invasive[8]. Switching toward the invasive state is often contributed by stresses in the tumor microenvironment, such as hypoxic condition, nutrient deprivation, or inflammatory response. This invasive phenotype can also be induced by various cytokines, including tumor necrosis factor, and transforming growth factor-beta (TGF-β)[4,8].

Cancer cells usually rewire their metabolism to match their increased energy and macromolecules demand during rapid cell proliferation, to adapt to nutrient scarcity and promote metastasis[13,14]. Lipids are one of the most important nutrients, not only as the main component of the cellular membrane, but also serve as energy source and storage, and play significant roles in signaling pathways, many of which are related to tumor progression, such as the phosphatidylinositol in PI3K/AKT/mTOR pathway[15,16]. Fatty acids (FAs) are shown to play significant roles in supporting melanoma aggressiveness, as both FA de novo synthesis and exogenous uptake are shown to be upregulated and support melanoma metastasis formation[17,18], or supporting survival

[1]Department of Organ Anatomy, Graduate School of Medicine, Tohoku University, 9F Building #5, 2-1 Seiryo-Machi, Aoba-ku, Sendai 980-8575, Japan. [2]Faculty of Medicine, Khon Kaen University, 123 Nai Muang, Muang 40002, Khon Kaen, Thailand. [3]Department of Anatomy, Tohoku Medical and Pharmaceutical University, 4-4-1 Komatsushima, Aobaku, Sendai, Miyagi 981-8558, Japan. ✉email: hmiyazaki@med.tohoku.ac.jp

during metastasis by certain FAs[19]. The degree of FA saturation partially determines melanoma phenotypes by inducing stress responses and altering membrane fluidity[20,21].

Fatty acid binding protein 7 (FABP7) is a fatty acid chaperon protein highly expressed in the brain and glial cells, which binds to long chain poly-unsaturated FAs (PUFAs), notably docosahexaenoic acid (DHA), regulates cell mobility during brain development via peroxisome proliferator-activated receptors (PPARs) activation[22,23], and facilitates myelination[24]. When FABP7 binds to DHA, it is transformed and relocated to the nucleus and activates PPAR-gamma (PPAR-γ), triggering multiple targets, including anti-inflammatory and neuroprotective genes[25–27]. Several cancers, including breast cancer, glioma, carcinomas, and melanomas, also express FABP7 with its expression associated with poor prognosis[28–31]. Ligand-bound FABP7 enhances glioma proliferation through various epigenetic mechanisms, such as via PPARγ, caveolae formation, or nuclear lipid droplet accumulation[30]. Additionally, FABP7 potentially supports glioblastoma cell survival from ROS in hypoxic condition by increasing lipid droplet formation, under regulation of hypoxia-inducible factor 1-alpha (HIF-1α)[32]. In melanoma, FABP7 expression is associated with tumor thickness, and enhances its proliferation, migration, and invasion[33–35].

But the aspects on melanoma's unique phenotypic plasticity and altered lipid metabolism have not yet been thoroughly explored. Our study's goal is to uncover how FABP7 promotes melanoma progression on the transcriptional and metabolic level, regarding fatty acids and lipid metabolism.

Results

FABP7 is highly expressed in B16F10 melanoma cells

FABP7 has been shown to be highly expressed in melanoma cells[34,36]. We confirmed a high *Fabp7* mRNA (Fig. 1a) and protein expression (Fig. 1b–d) in highly metastatic murine melanoma cell line B16F10 in comparison with its lowly metastatic B16F1 counterpart[37]. Immunocytochemistry staining revealed a homogeneous FABP7 expression both in the cytosol and the nucleus (Fig. 1d). Subcutaneous and intravenous B16F10 cells in vivo transplantation also expressed FABP7 (Fig. 1e). Interestingly, we found that FABP7 expression of the tumor foci in the lungs from the intravenously transplanted mice was relatively higher than those of the subcutaneous transplants.

Loss of FABP7 increases B16F10 invasiveness

A *Fabp7* knockout (KO) B16F10 cell line was generated using CRISPR/Cas9 splicing system. The knockout mutation was detected in DNA sequence. The complete knockout was confirmed by quantitative real-time polymerase chain reaction (qRT-PCR), western blot, and immunofluorescent staining, showing a stable absence of FABP7 protein expression (Fig. 2a–c).

While loss of FABP7 did not affect the proliferation rate of these cells (Fig. 2d), *Fabp7*-KO cells showed an increase in both migration and invasion (Fig. 2e,f), with twofold higher invaded cell number in the KO group ($p = 0.002$). *Fabp7* knockdown by siRNA interference (Fig. 2g,h) also showed a similar trend of enhanced invasion, (Fig. 2j,k) with almost sixfold higher invaded cells ($p < 0.001$). Unexpectedly, the wound closure rate was slower in the knockdown cells in contrast to the KO system (Fig. 2j). Taken together, these results showed a trend that loss of FABP7 promote B16F10 invasion without effects on proliferation in vitro.

Loss of FABP7 decreases tumor growth but increases in vivo *lung metastasis formation*

Control (CT) and *Fabp7*-KO B16F10 cells were implanted subcutaneously on C57BL/6 mice to evaluate in vivo effects ($n = 13$ for each group). Tumor formation started to be visible at day 4–5 after injection and the KO groups were significantly smaller in size (Fig. 3a,b), with less than half of the CT group at day 15 after injection (Fig. 3c, $p = 0.002$).

To evaluate the ability to form metastasis, the same cell lines were intravenously injected into the tail veins of C57BL/6 mice ($n = 8$ for CT, and $n = 9$ for KO). The mice's body weight and behavior were monitored daily, until 14 days after injection, when we sacrificed the animals and harvested the lungs to evaluate for metastatic formation.

Multiple melanotic foci appeared on the lungs in both CT and KO groups. The foci count of KO group was significantly higher than CT, yet the size of each metastatic foci noticeably smaller (Fig. 3d,e).

Fabp7 knockout alters cellular lipid composition

Cellular lipid content of *Fabp7*-KO B16F10 cells was evaluated with liquid chromatography–mass spectrometry (LC–MS/MS) lipidomics (Supplementary Data 1). Phosphatidylcholines, diacylglycerides, and phosphatidylethanolamines were the highest lipid composition in both groups (Fig. 4a). We found an overall increase of glucosyl ceramide, lysophosphatidylethanolamine, and phosphatidic acid species in the KO group, while a decrease in monoglycerides, gangliosides, sphingosines, acylcarnitine lactosyl ceramides, and cardiolipins could be observed. Among free fatty acids (FA), arachidonic acid (FA(20:4)) was the predominating FA, following by oleic acid (FA(18:1)), dihomo-gamma-linolenic acid (FA(20:3)), and stearic acid (FA(18:0)) (Fig. 4b). A significant decrease of stearic acid (FA(18:0), $\log_2FC = -1.663$, $p = 0.003$), α-linolenic acid (FA(18:3), $\log_2FC = -1.242$, $p = 0.003$), arachidonic acid (FA(20:4), $\log_2FC = -1.700$, $p = 0.032$), and docosapentaenoic acid (FA(22:5), $\log_2FC = -2.580$, $p = 0.040$)) can be observed in KO group.

We found a significant correlation between the abundance of lipids and the number of double bonds. There was an overall decrease in lipid species with higher double bond number within the KO group (Fig. 4c,d). This trend was also present when considering specific lipid groups, including phosphatidylcholines and glycerolipids, but not apparent for FAs (Fig. 4e,f). In other words, the saturated to unsaturated ratio in structural and storage lipids was higher in the KO cells and may represent the altered fatty acid metabolism and transportation.

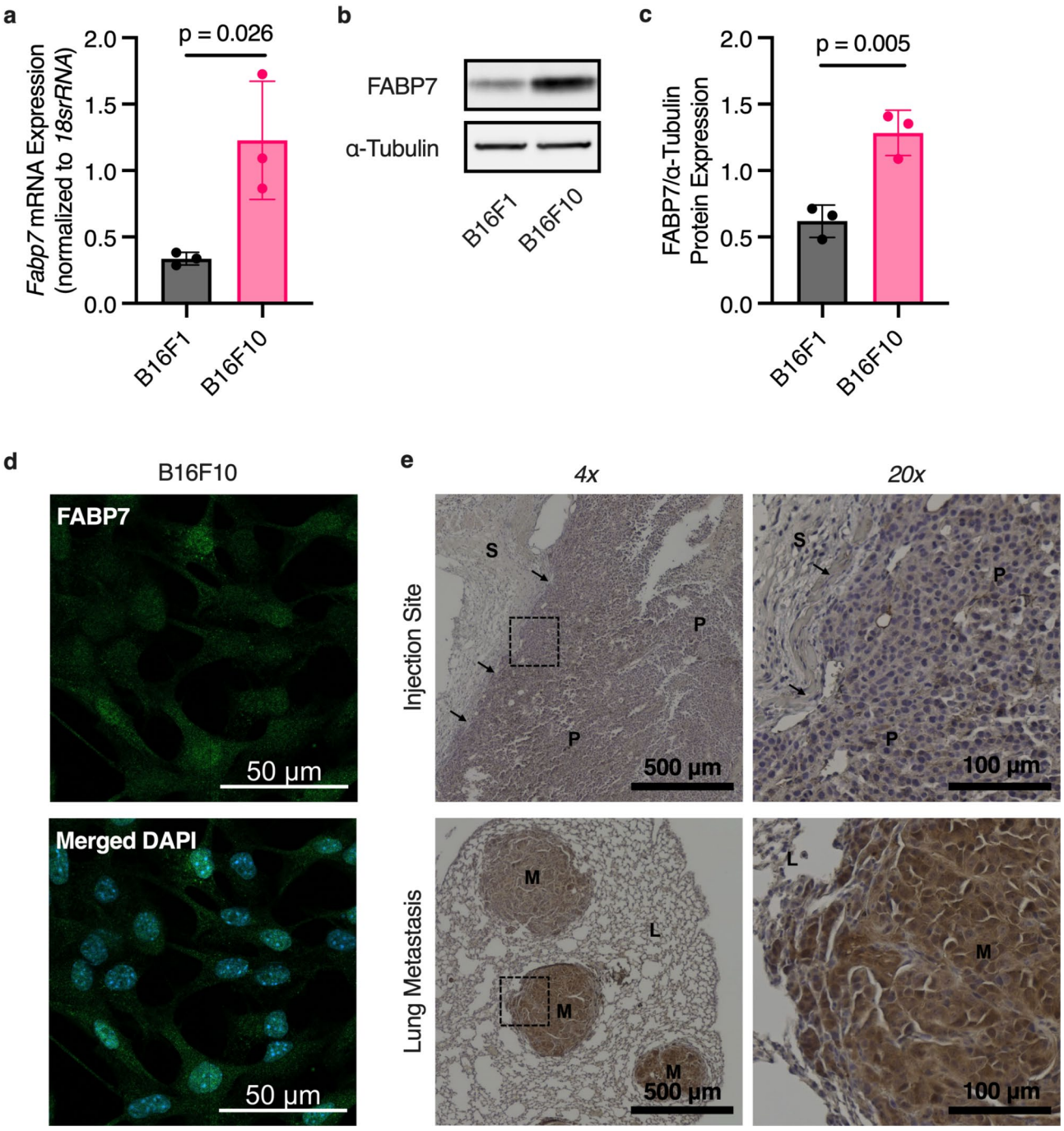

Fig. 1. FABP7 is highly expressed in B16F10 murine melanoma. (**a**) qRT-PCR analysis of *Fabp7* expression in B16F1 and B16F10 cell line, normalized to *18srRNA*. (**b**) Western blot analysis of FABP7 of B16F1 and B16F10 cell lines. (**c**) FABP7 protein expression of B16F1 and B16F10 cell lines from western blot analysis, normalized to alpha-tubulin. Original blots are presented in Supplementary Fig. 1 d Immunofluorescent analysis of FABP7 protein expression in B16F10 cells with or without DAPI nuclear counterstain. e DAB staining of FABP7 in mice tissue transplanted with B16F10 cells. The top row is from the primary tumor at the subcutaneous injection site with arrows show the border between the primary tumor (P), and subcutaneous tissue (S). The bottom row shows metastatic tumor foci (M) within normal lung tissue (L) from intravenous tumor injection. Right panels are magnification from the dotted square regions. Scale bar represents 500μm and 100μm for left and right panels respectively. Graphs show mean ± s.d. from at least three independent experiments. Unpaired t-test.

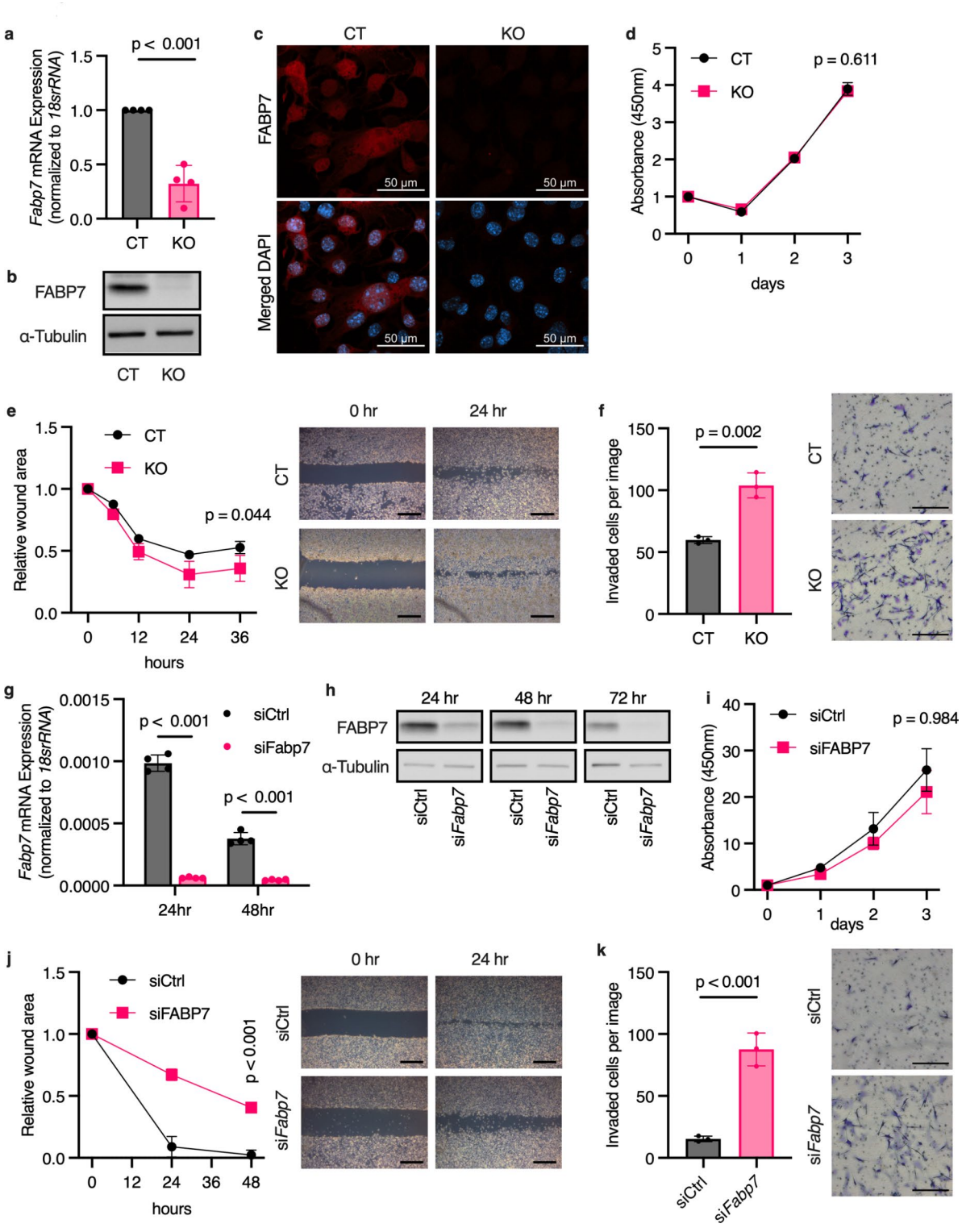

Fabp7 knockout causes phenotypic shift toward invasive profiles

An increase in *Axl* mRNA expression in the KO cell line was observed, while *Mitf* expression did not significantly change but remained at the original low level, corresponding to the $Mitf^{Low}/Axl^{High}$ invasive phenotype (Fig. 5a). TGF-β signaling is related to the invasive phenotype of melanoma cells[8], and we indeed found an increased mRNA expression of TGF-β receptors *Tgfbr1*, *Tgfbr2*, and *Tgfbr3* in the KO cells (Fig. 5b). It is known that TGF-β signaling induces invasiveness of epithelial cancers thorough epithelial-to-mesenchymal transition (EMT)[38]. We found that certain EMT marker mRNAs were upregulated in the KO cells, including *Cdh2* and *Zeb2* (Fig. 5c). Changes in these genes suggest a transcriptional rewiring toward the more invasive, de-differentiated phenotype. We also discovered a higher reactive oxygen species (ROS) content in KO cells when peroxides were introduced (Fig. 5d), suggesting an impairment in ROS elimination.

◂**Fig. 2**. Loss of FABP7 increases B16F10 invasiveness in vitro. (**a**) qRT-PCR analysis of *Fabp7* mRNA expression in CRSPR/Cas9 *FABP7* knockout B16F10 cell line in comparison with control cell line, normalized to *18srRNA*. (**b**) Western blot analysis of *Fabp7*-KO B16F10 cell line (KO), in comparison with control cell line (CT). Original blots are presented in Supplementary Fig. 2 c Immunofluorescent analysis of FABP7 protein expression in *Fabp7*-KO B16F10 cell line (KO), in comparison with control cell line (CT), with or without DAPI nuclear counterstain. (**d**) Proliferation assay of *Fabp7*-KO B16F10 cell line (KO), cultured in complete medium with 10%FBS, in comparison with control cell line (CT). (**e**) Scratch wound healing assay of *Fabp7*-KO B16F10 cell line (KO), in comparison with control cell line (CT). Graph shows the wound area relative to the time of the scratch, with representative imaged on the right. Scale bar = 1,000µm. (**f**) Invasion assay of *Fabp7*-KO B16F10 cell line (KO), in comparison with control cell line (CT), through the GelTrex® precoated Boyden chamber, using 10%FBS as chemoattractant, with representative imaged on the right. Scale bar = 100µm. g qRT-PCR analysis of *Fabp7* mRNA expression in *Fabp7* knockdown B16F10 cells using siRNA (si*Fabp7*), in comparison with control cells (siCtrl), normalized to *18srRna*, at 24 and 48 h after transfection. (**h**) Western blot analysis of si*Fabp7* knockdown B16F10 cells in comparison with control cells (siCtrl) at 24, 48, and 72 h after transfection. Original blots are presented in Supplementary Fig. 3. (**i**) Proliferation assay of si*Fabp7* knockdown B16F10 cells in comparison with control cells (siCtrl). (**j**) Scratch wound healing assay of si*Fabp7* knockdown B16F10 cells in comparison with control cells (siCtrl) with representative imaged on the right. Scale bar = 1,000µm. k Invasion assay of si*Fabp7* knockdown B16F10 cells in comparison with control cells (siCtrl) through the GelTrex® pre-coated Boyden chamber, using 10% FBS as chemoattractant, with representative imaged on the right. Scale bar = 100µm. Graphs show mean ± s.d. from at least three independent experiments. Unpaired t-test and multiple t-test corrected for 1% FDR.

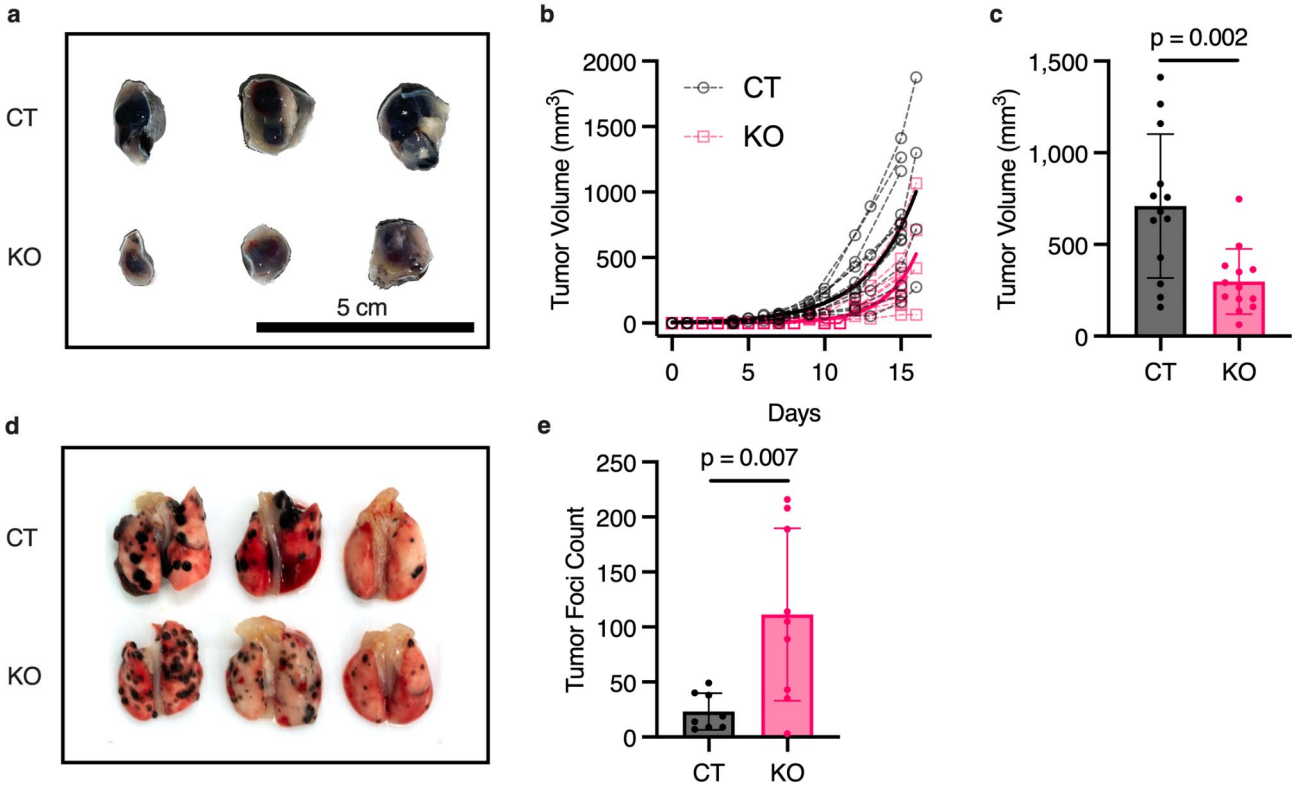

Fig. 3. Loss of FABP7 decreases primary tumor growth but increases in vivo lung metastasis formation. (**a**) Primary tumor dissected from the subcutaneous injection site at day 16 after transplantation. Top row is the control group (CT), and bottom row is the knockout group (KO). (**b**) Estimated tumor volume over time of the subcutaneous injection with CT and KO cells. Connecting dots represent individual mice. Thick lines represent the exponential curve fit for each group. (**c**) Comparison of tumor volume at day 15 after subcutaneous injection with CT and KO cells. (**d**) Lungs harvested from the intravenous injection model, showing black spots of tumor metastatic foci. Top row is the CT group, and bottom row is the KO group. (**e**) Count of lung metastatic tumor foci from the intravenous injection model. Graphs show mean ± s.d. Unpaired t-test.

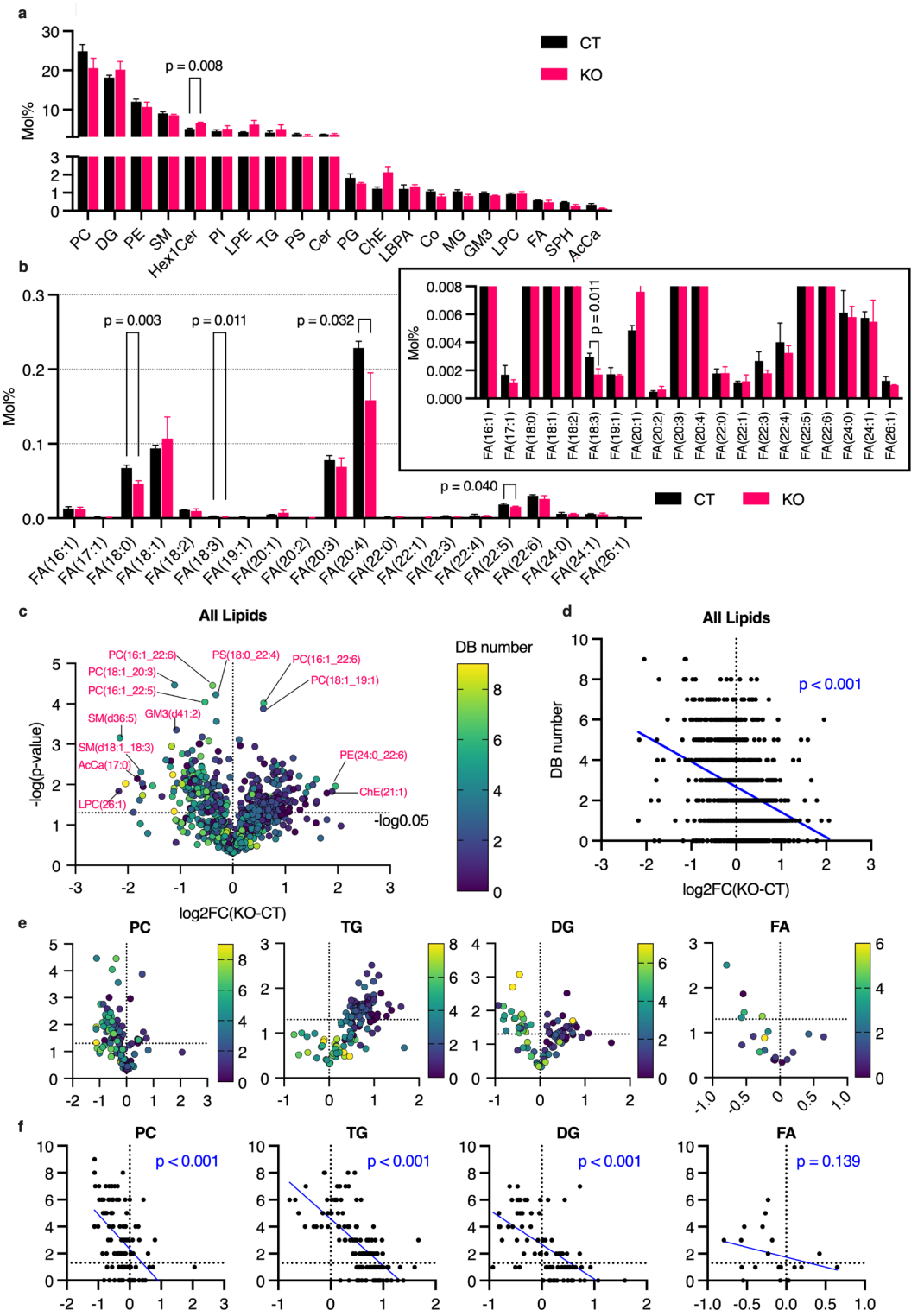

Discussion

Several studies have demonstrated the roles of FABP7 in promoting aggressiveness of cancers, including melanomas, by supporting tumor growth and metastatic process. We discovered for the first time, FABP7's role in regulating melanoma phenotypic shift, using a combination of in vitro experiments, an animal model, and metabolomic analysis.

FABP7 was originally found to be highly expressed in the brain, remarkably in astrocytes and other glial cells. Since melanomas originate from the neural crest cell-derived melanocytes, they may retain the high FABP7 expression from their origin. Goto, et al., demonstrated that *FABP7* mRNA copies are higher in the primary melanoma, than the metastatic site[34]. While patient-acquired tissue immunohistochemistry by Slipicevic, et al. revealed highest FABP7 expression in benign nevi lesion, followed by primary and metastatic melanomas at

◀**Fig. 4**. *Fabp7* knockout alters cellular lipid composition. (**a**) Lipidomics analysis of *Fabp7*-KO (KO) and control (CT) B16F10 cells, showing ratio of each of the top 20 most abundant lipid species in mol-percent of total lipid. (**b**) Ratio of each free fatty acids to total lipid of KO and CT cells, with scaled up graph in the box. (**c**) Volcano plot of lipidomics analysis result, considering the relationship between number of double bonds in each lipid species, and overall fold change of *Fabp7*-KO over CT B16F10 cells. Each dot represents a specific lipid species with color indicating the total number of double bonds from no double bond in dark purple, to highest number of double bonds in light yellow. X-axis represents the $\log_2$ fold change (FC) of KO over CT. Y-axis represents the statistical significance for each pair, showing in -log(p-value). Top few significant, highest rank (calculated from -log(p-value) $\times|\log_2 FC|$) lipids are labelled in red. Horizontal dashed line represents the cut point of p-value = 0.05. (**d**) XY correlation graph from Fig. 4c, showing a negative correlation between the fold change from KO to CT (x-axis) and the double bond number (y-axis). Blue line represents simple linear curve fit. P-value represents significant deviation from zero. (**e**) Volcano plots of lipidomics analysis result, considering the relationship between number of double bonds and fold change of *Fabp7*-KO over CT B16F10 cells in specific groups of lipids. X-axis represents the $\log_2$ fold change (FC) of KO over CT. Y-axis represents the statistical significance for each pair. Horizontal dashed line represents the cut point of p-value = 0.05. (**f**) XY correlation graph from Fig. 4e. Bar graphs show mean ± s.d. from three separate samples. PC, phosphatidylcholine, DG, diglyceride, PE, phosphatidylethanolamine, SM, sphingomyelin, Hex1Cer, glucosyl ceramide, galactosyl ceramide, PI, phosphatidylinositol, LPE, lysophosphatidylethanolamine, TG, triglyceride, PS, phosphatidylserine, Cer, ceramide, PG, phosphatigylglycerol, ChE, cholesteryl ester, LBPA, bis(monooleoylglycero)phosphate, Co, coenzyme Q, MG, monoglyceride, GM3, gangliosides, LPC, lysophosphatidylcholine, FA, free fatty acid, SPH, sphingosine, AcCa, acyl carnitine, LPI, lysophosphatidylinositol, LPG, lysophosphatidylglycerol, Hex2Cer, lactosyl ceramide, Ch, cholesterol, CL, cardiolipin, PA, phosphatidic acid, LPS, lysophosphatidylserine, ZyE, zymosterol ester. Unpaired t-test was used to compare each lipid species.

similar levels[35]. These fluctuations hint that FABP7 may be downregulated during the malignant transformation and metastatic processes, either as metastasis initiator, or as a result from metastatic processes.

We found relatively higher FABP7 expression in high-metastatic B16F10 murine melanoma cells compared to B16F1, the low-metastatic variant[39,40]. Our finding may appear contradictory to the results from patient tissue studies. However, FABP7 expression in cell lines was observed in vitro, in a stable state, therefore, it cannot represent in vivo fluctuations. Nonetheless, it is plausible that high FABP7 expression supports B16F10 invasiveness. Our in vivo models also showed a relatively higher FABP7 expression in the lungs, than at the primary tumor site, which may be due to a different metastatic process and could not represent the naturally occurred metastasis which involves multiple steps, since our method involved direct injection of tumor cells into the bloodstream. The strong FABP7 expressing metastatic foci in our model could be explained by ROS scavenging capacity. Direct exposure to blood stream can be stressful to melanoma cells and lead to reactive oxygen species-induced cell death[19], which could be attenuated by lipid droplets[41]. Bansaad, et al., had shown that FABP3 and FABP7 protect glioblastoma cells from ROS during hypoxia-reoxygenation by enhancing lipid droplet formation[32], it is reasonable that melanoma cells with higher FABP7 expression will similarly survive better in harmful environment then successfully form tumor foci at distant sites.

In our study, *Fabp7*-KO B16F10 cells had higher capability to invade through ECM-coated membrane without noticeable change in proliferation, contradicting to other studies which showed decreased melanoma proliferation, migration, and invasion in absence of FABP7[33,35]. Our results showed slower primary tumor growth in *Fabp7*-KO group, suggesting its importance in cell proliferation in vivo. Presence of complex tumor microenvironment and available nutrients may account for the different findings from in vitro experiments. Higher tumor foci count in the lungs of *Fabp7*-KO group corresponds to the increased invasiveness found in trans-well experiments, but the size of metastatic foci was smaller than the WT group. This, once again, supports its role in tumor proliferation, which might also be mitigated in KO group, leading to slower tumor growth despite successfully forming a metastatic focus. Still, a similar deterioration was not apparent in in vitro results. It is very likely that the TME can dramatically affect the outcome. Since melanoma is a solid tumor of cells forming in a spheroid mass, each tumor cells may be affected by the environment differently. For example, cells at the tumor core may be less exposed to nutrients or oxygen than those at the periphery, especially in rapidly growing tumor without sufficient vascularization[42]. With limited nutrients, tumor cells will have to switch to different modes of metabolism, such as using lipids as main source of energy, instead of glucose[43]. Therefore, *Fabp7*-KO cells with impaired fatty acid transportation, would be susceptible to such metabolic stress, halting their proliferation or undergoing apoptosis, leading to an overall smaller tumor size. This locational nutrient availability is likely not present in monolayer cell culture format. Additionally, other TME components, including immune cells, fibroblasts, adipocytes, and various ECM molecules and cytokines, further complicate the tumor progression[44–46].

Since FABP7 prefers PUFAs as its ligand[23], *Fabp7*-KO cells presumably have impaired uptake and transportation of these fatty acids, leading to lower overall amount of unsaturated fatty acids and eventually, increasing the saturated to unsaturated lipid ratio. Imbalance between saturated (SFA) and unsaturated fatty acids can affect cell behaviors[20,47]. Cell membrane which incorporates unsaturated fatty acids has higher fluidity, enhancing cell motility during invasion, while excessive cellular SFAs can lead to ER stress, unfolded protein response, and ceramide formation[21]. These conditions can activate cellular stress signaling and eventually induce phenotypic shifting toward the invasive phenotype[48]. The evidence of lipid saturation change was only apparent in incorporated lipids, but not free fatty acids (FFAs), suggests the role of FABP7 as FA transporter since FFAs

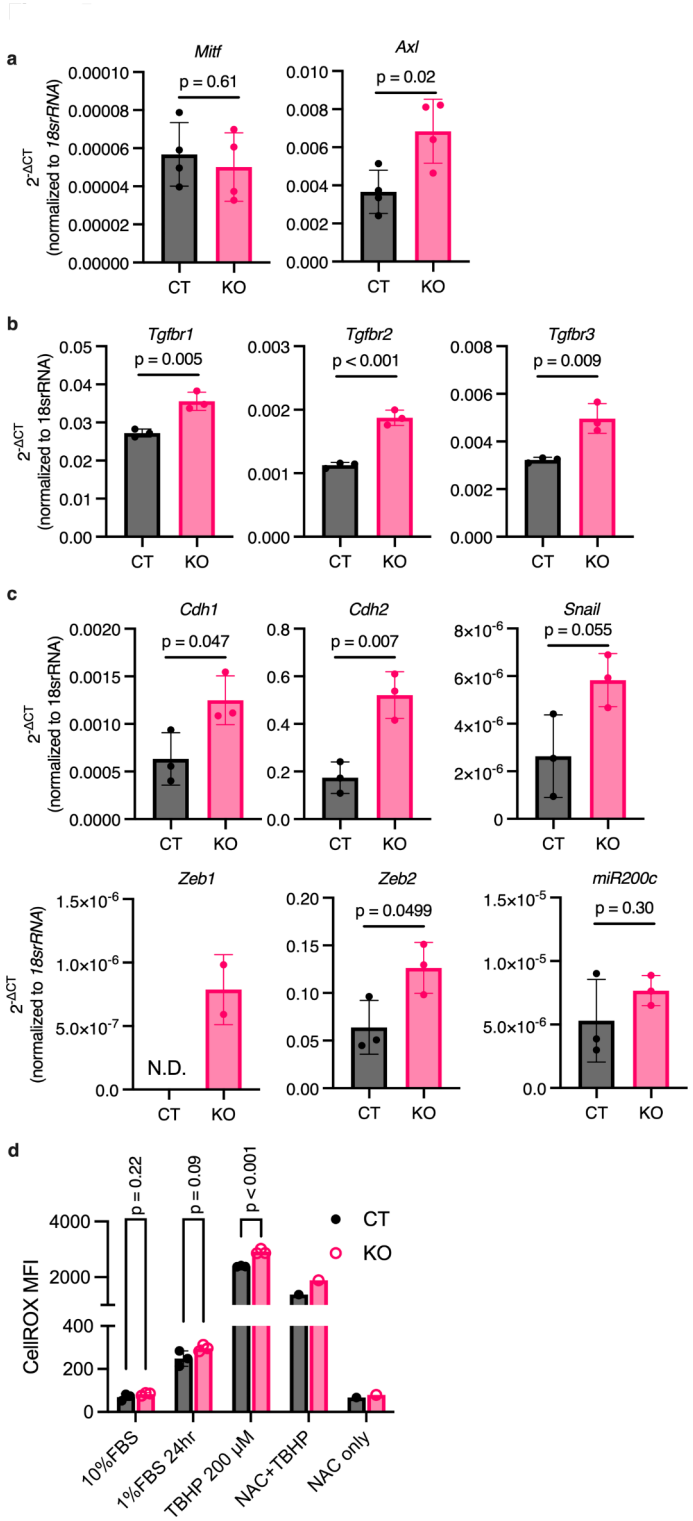

Fig. 5. *Fabp7* knockout causes phenotypic shift toward invasive profiles. (**a**) qRT-PCR analysis of *Mitf* and *Axl* mRNA expression in *Fabp7*-KO B16F10 cell line (KO) in comparison with control cell line (CT), normalized to *18srRNA*. (**b**) qRT-PCR analysis of TGF-β receptors mRNA expression in *Fabp7*-KO B16F10 cell line (KO) in comparison with control cell line (CT), normalized to *18srRNA*. c qRT-PCR analysis of convention epithelial-to-mesenchymal transition genes in *Fabp7*-KO cell line (KO) in comparison with control cell line (CT), normalized to *18srRNA*. (**d**) Mean fluorescence intensity (MFI) measured by flow cytometry, of CellROX green fluorescence staining for reactive oxygen species (ROS) in CT and KO cells in normal condition (10%FBS), serum deprived condition (1%FBS), treated with tert-Butyl hydroperoxide (TBHP), TBHP with N-acetylcysteine (NAC), and NAC alone. Graphs show mean ± s.d. from at least three independent experiments. Unpaired t-test. N.D., not detected.

may be regulated by other entities. Considering FABP7's binding affinity toward specific FAs, the reduction of arachidonic acid (AA) in *Fabp7*-KO cells is not unexpected. As AA is the precursor of multiple inflammatory cytokines that benefit tumor growth[49], a lower level of this FA could hinder tumor growth at primary site as well as at metastatic foci.

We found evidence of phenotypic shifting in KO cells, characterized by an increase in *Axl* expression and various EMT markers. While there is no change in *Mitf*, its original expression is very low in the wild type cells and remains low in the KO cells, resulting in the invasive $Mitf^{Low}/Axl^{High}$ signature.

Among multiple factors that can influence the phenotypes, TGF-β signaling is a well-studied pathways known to induce invasion and de-differentiation[8]. KO cells have higher expression of TGF-β receptors, therefore, an increase in TGF-β signaling could be expected. Kagawa, *et al*[30,50], showed that FABP7 regulates caveolin-1 (Cav-1) expression in gliomas and astrocytes. Apart from changes in membrane FA component that determine the lipid raft function, Cav-1 also plays a significant role in membrane lipid raft formation and can inhibit TGF-β/SMAD signaling via the TGF-β type I receptor[51]. As a result, these receptors may be disinhibited in *Fabp7*-KO cells, leading to increased TGF-β signaling.

In epithelial cancers, TGF-β signaling is also known to induce EMT by formation of SMAD complex that binds to DNA[38]. Different markers used in this study were expressed at different stages of the transition. In brief, epithelial tumor cells generally express *CDH1* which codes for E-cadherin, the main component of cell–cell adhesion proteins in tight junctions, that maintain the integrity of epithelial tissue[52]. *CDH2*, on the other hand, codes for N-cadherin, which is upregulated in mesenchymal stage, associated with cancer invasiveness[53].

Cdh2 was upregulated in *Fabp7*-KO cells, hinting the mesenchymal-like transition. Meanwhile, upregulation of the epithelial gene *Cdh1* was also observed, suggesting a partial EMT-like transformation, that may support the transition back to the proliferative phenotype after successful metastatic seeding[54]. ZEB1 and ZEB2 are transcription factors that repress E-cadherin expression, eventually promoting the mesenchymal transition[55]. Thereby, *Zeb2* mRNA upregulation in *Fabp7*-KO cells can also account for the enhanced invasiveness.

Essentially, changes in these genes indicate that FABP7 can regulate melanoma aggressiveness by preventing it from shifting into the invasive phenotype. This regulation occurs both through direct alterations of structural FA components and indirectly through TGF-β and stress signaling, which lead to EMT-like transitioning alongside the phenotypic shift.

Out of many mechanisms underlying cell stress response, oxidative stress is one of the most common and ubiquitous stress inducers in most type of cells, and most importantly, it can promote tumor growth and metastasis through various mechanisms[56]. Our preliminary result shows a trend of ROS accumulation in *Fabp7*-KO cells under ROS treatment, but not in ROS-inducing, serum-deprived condition (Fig. 5d), suggesting an impaired ROS elimination in KO cells, rather than higher ROS production. These findings are explainable by the role of FABP7 as ROS scavenger, reducing oxidative stress by means of lipid droplets[57]. Therefore, oxidative stress could also be one of the underlying mechanisms of phenotypic shift and invasiveness.

In conclusion, this study explores the roles of FABP7 concerning melanoma phenotypic plasticity and lipid metabolism. FABP7 plays an important role in regulating the balance of lipid saturation by preserving unsaturated FA (UFA) levels within the cell. In the absence of FABP7, saturated FA (SFA) to UFA ratio increases, likely triggering stress responses and eventually the phenotypic shift toward the invasive phenotype. Through this mechanism, melanoma cells acquire higher metastatic capability, but with a reduction in primary tumor growth. These insights could be potential for finding candidates regarding lipid metabolism, and development of better melanoma therapies.

Materials and methods

Reagents and antibodies

Reagents and antibodies used in this experiment are as followed: Dulbecco's modified Eagle's medium (Sigma Aldrich, Co.), Fetal bovine serum (Sigma Aldrich, Co., Lot# BCBX4307) Penicillin–Streptomycin Mixed Solution (Nacalai Tesque, Kyoto, Japan), 2.5% Trypsin (Thermo Fisher Scientific Inc.), Normal goat serum (Jackson Immuno Research Labs), Bovine serum albumin (BSA) (Wako, Japan), DAPI nucleic acid stain (Invitrogen, Ltd.). Primary antibodies included anti-mouse FABP7 rabbit polyclonal IgG established by our laboratory[58], and anti-alpha-tubulin rat monoclonal IgG (Santa Cruz Biotechnology Cat# sc-53029, RRID:AB_793541). Secondary antibodies used in this study were Alexa Fluor® 488 goat anti-rabbit IgG (H + L) (Thermo Fisher Scientific Cat# A-11070, RRID:AB_2534114), Alexa Fluor® 568 goat anti-rabbit IgG (H + L) (Thermo Fisher Scientific Cat# A-11011, RRID:AB_143157), horseradish peroxidase (HRP) conjugated goat anti-rabbit IgG H&L (Abcam Cat# ab6721, RRID:AB_955447), and HRP conjugated goat anti-rat IgG (Millipore Cat# AP136P, RRID:AB_11214444).

Animals

8–12 weeks old wild type male and female C57BL/6J mice (RRID:IMSR_JAX:000,664) were obtained from the Tohoku University Graduate School of Medicine Animal Center. All animal experiments were approved by the Ethics Committee for Animal Experimentation of Tohoku University Graduate School of Medicine and carried out according to the Guidelines for Animal Experimentation of the Tohoku University Graduate School of Medicine and under the law and notification requirements of the Japanese government. All animal experiments were conducted in accordance with the ARRIVE guidelines (Animal Research: Reporting of In Vivo Experiments).

Cell cultures

Murine melanoma cell lines B16F1 (NCI-DTP Cat# B16F1, RRID:CVCL_0158) and B16F10 (NCI-DTP Cat# B16F10, RRID:CVCL_0159) were obtained from Cell Resource Center for Biomedical Research, Tohoku

University. All cell lines were maintained in DMEM supplemented with 10% (v/v) heat-inactivated FBS, 1% (v/v) penicillin/streptomycin, and 2 mM l-glutamine, at 37 °C, 5% CO_2 unless specified otherwise. All cell culture experiments were performed under strict sterile condition.

Generation of CRISPR/Cas9 Fabp7 knockout cell line

CRISPR/Cas9 *Fabp7* knockout B16F10 cells were generated as previously described[33,59]. Briefly, sgRNA expression plasmid, we selected target sites within exon 1 of murine *Fabp7* gene using CHOPCHOP software (https://chopchop.cbu.uib.no/). The following oligonucleotide was used: gRNA; 5'-TAGATGCTTTCTGCGC AACCTGGA-3' sequence of exon 1. The double-stranded oligonucleotide was synthesized and inserted into pGuide-it-ZsGreen1 vector (Takara, Tokyo, Japan) following manufacturer's protocol. The constructed vector was transfected into B16F10 cells using Lipofectamine® 2000 Reagent (Thermo Fisher Scientific Inc.). The culture medium was changes 6 h after transfection. 48 h after transfection, cells were collected and selected for green fluorescence expressing cells with flow cytometry using BD FACS Aria II (Becton Dickinson, Japan), and seeded as single cells per well in 96-well plates. Cell clones were cultured and propagated in DMEM with 10% FBS at 37 °C, 5% CO_2, passaged and stocked at appropriate time. Complete knockout of FABP7 was confirmed with DNA sequencing analysis, and absence of *Fabp7* mRNA protein expression by qRT-PCR, western blotting, and immunofluorescent staining.

siRNA gene silencing

B16F10 cells were transfected with a stealth siRNA targeting Fabp7 (Cat# MSS202379, Thermo Fisher Scientific Inc.) and negative control siRNA (Cat# sc-37007, Santa Cruz Biotechnology, CA.), using Lipofectamine® RNAiMAX reagent (Thermo Fisher Scientific Inc.) following the manufacturer's protocol. After optimization, knockdown of Fabp7 mRNA and FABP7 protein expression were confirmed with qRT-PCR and western blot analysis at 48 h after transfection.

Cell proliferation assay

Cells were seeded at 5×10^3 cells/well in 24-well plates and cultured in DMEM with 10% FBS at 37 °C, 5% CO_2 overnight. Cell proliferation was assessed using Cell Count Reagent SF (Nacalai Tesque, Kyoto, Japan) according to the company protocol, every 24 h for at least 72 h. The reagents were transferred into 96-well plates to be read at 450 nm wavelength with Multiskan FC microplate photometer (Thermo Fisher Scientific Inc.).

Scratch wound healing assay

Cells were seeded in 6-well plates and cultured in DMEM with 10% FBS at 37 °C, 5% CO_2 until near confluency. Media were replaced with 0.5% FBS DMEM and cultured for another 24 h to minimize cell proliferation. Scratch wounds were introduced with a 200 µL pipette tip directly onto the confluent cell monolayer. The images of the wound were taken at four different locations per well. The wound sizes were measured using Zeiss Zen Lite software, by drawing a polygon shape over the wound relative to a marker made on the culture plate, then record the polygon area as wound size (in μm^2). The wound sizes were measured at the same locations every 12–24 h until 72 h or complete closure. Cell migration was assessed by the reduction percentage of the wound size over time.

Boyden's chamber invasion assay

Cells were cultured in DMEM with 10% FBS overnight, then the media were replaced with DMEM with 1% FBS and cultured for another 6 h. Serum-deprived cells were collected by trypsinization and plated into 24-well plates with 8.0 µm polyester membrane cell culture inserts pre-coated with Geltrex™ Basement Membrane Matrix (Thermo Fisher Inc.). The top chambers contained 2×10^5 cells in DMEM with 1% FBS, while the bottom chambers contained DMEM with 10% FBS as chemoattractant. The plates were incubated in 37 °C, 5% CO_2 for 24 h, then the inserts were fixed with 4% PFA and stained with 0.1% crystal violet. Images of the membrane were taken randomly at four different locations per sample. The invaded cells were counted under microscope and calculated as cells per image.

RNA extraction and quantitative real-time PCR (qRT-PCR)

RNA templates from cell culture were isolated using RNeasy Micro Kit (QIAGEN) following the manufacturer's protocol. cDNA synthesis was performed with GeneAce cDNA Synthesis Kit (Nippon Gene, Tokyo, Japan). qRT-PCR was performed using Applied Biosystems 7500 Real-Time PCR System (RRID:SCR_018051) with THUNDERBIRD® Next SYBR® qPCR Mix (Toyobo Inc.). RNA expression was quantified by normalizing cycle threshold (C_T) values with 18s ribosomal RNA expression and analyzed by comparative ΔC_T method. The primer sequences are shown in Table 1.

Western blotting

Cells were lysed in Pierce™ RIPA buffer (Thermo Fisher Scientific Inc.) with cOmplete Mini protease and phosphatase inhibitor cocktails (Roche) for at least 30 min on ice with gentle agitation, ultrasonicated, and centrifuged. The supernatants were collected and measured for protein concentration using the BCA assay (Thermo Fisher Scientific Inc.). Western blot samples were mixed with Laemmli buffer to the final protein concentration of 1–2 g/mL, incubated at 95 °C for 5 min, and stored at -20 °C until gel electrophoresis.

Protein samples were resolved in 10% or 12% TGX Stain-Free FastCast Acrylamide Kit (Bio-Rad), transferred onto Immobilon-P PVDF membrane (Sigma Aldrich, Co.), blocked with 5% BSA in 0.1% Tween-20 Tris-Buffered Saline, and incubated in primary antibody at 4 °C overnight with gentle agitation. Then, membranes were incubated in HRP-conjugated secondary antibody of appropriate hosts at room temperature for 60 min.

Gene	Strand	Sequence
18srRNA	Forward	GTAACCCGTTGAACCCCATT
	Reverse	CCATCCAATCGGTAGTAGCG
Axl	Forward	GGAGGAGCCTGAGGACAAAGC
	Reverse	TACAGCATCTTGAAGCCAGAGTAGG
Cdh1	Forward	CATCATTGAGAGGGAGACAG
	Reverse	GACACGGCATGAGAATAGAG
Cdh2	Forward	CTGACTGAGGAGCCTATGAA
	Reverse	CAGTCTCTCTTCTGCCTTTG
Fabp7	Forward	AAGTGGGAAACGTGACCAAAC
	Reverse	CAACCGAACCACAGACTTACAG
miR200c	Forward	GTCTTACCCAGCAGTGTTTG
	Reverse	TACCCGGCAGTATTAGAGAC
Mitf	Forward	AGATTTGAGATGCTCATCCCC
	Reverse	GATGCGTGATGTCATACTGGA
Snail	Forward	CAACTATAGCGAGCTGCAGGA
	Reverse	GTACCAGGAGAGAGTCCCAGAT
Tgfbr1	Forward	TCTGCATTGCACTTATGCTGA
	Reverse	AAAGGGCGATCTAGTGATGGA
Tgfbr2	Forward	CCGCTGCATATCGTCCTGTG
	Reverse	AGTGGATGGATGGTCCTATTACA
Tgfbr3	Forward	GGTGTGAACTGTCACCGATCA
	Reverse	GTTTAGGATGTGAACCTCCCTTG
Zeb1	Forward	CCAGCAGACCAGACAGTATT
	Reverse	TCTGAGTCACACACTCGTTGTC
Zeb2	Forward	GCCACGAGAAGAATGAAGAG
	Reverse	CTCCTTGGGTTAGCATTTGG

Table 1. Primers used for qRT-PCR.

The chemiluminescent signals were activated with ECL reagents and imaged with BioRad ChemiDoc Touch Imaging System (RRID:SCR_021693). Alpha-tubulin was used as protein reference. Signals were measured and analyzed with Image Lab Software v6.1 (http://www.bio-rad.com, RRID:SCR_014210).

Immunocytochemistry

Cells were seeded on poly-L-lysine coated 12mm glass cover slips in 24-well plates. Cells were fixed with 4% paraformaldehyde solution, permeabilized with 0.1% Triton X-100, blocked with 5% BSA, and incubated in primary antibodies at 4 °C overnight. After that, cells were washed and incubated with fluorescent-labelled secondary antibodies at room temperature for 60 min, with DAPI for nuclear counterstain then mounted with Fluoromount (Sigma-Aldrich, Co.) and kept at 4 °C in the dark until imaging with Zeiss LSM 800 with Airyscan Microscope (RRID:SCR_015963). Fluorescent signals were optimized and analyzed using Zeiss Zen Lite (https://www.zeiss.com, RRID:SCR_023747) and ImageJ v1.53t (https://imagej.net/, RRID:SCR_003070).

In vivo *tumor models*

Control and *Fabp7*-KO B16F10 cells were cultured in DMEM with 10% FBS and passaged at least two times before harvesting by trypsinization. 2×10^5 cells in 100 µL phosphate buffer solution (PBS) of control or *Fabp7*-KO B16F10 cells were subcutaneously injected into the right flank of the mice. Tumor sizes were measured using a caliper every 3 days for at least two weeks or until the maximum size reached 20 mm. Tumor volume was calculated by the formula: Volume (mm^3) = 0.5 × Length (mm) × Width ($mm)^2$. For the metastasis model, 2×10^5 cells in 100 µL PBS solution of control or *Fabp7*-KO B16F10 cells were injected into the tail vein of the mice. Mice's body weight and well-being were monitored closely for 14 days, until sacrificed. For tissue harvest, mice were adequately anesthetized with isoflurane inhalant, and maintained on the surgical plane of anesthesia throughout the whole sacrifice process. The mice's chest cavity was opened perfused intraventricularly with normal saline solution then perfused with 4% (PFA) solution. Mice were confirmed death with cervical dislocation while under deep anesthesia. The tumor and the lungs were harvested and fixed in 4% PFA further at 4 °C overnight, then processed for paraffinization.

Tissue paraffinization and immunohistochemistry

Fixed tissue samples were washed twice in PBS, then dehydrated through serial ethanol, cleared with xylene, and embedded in paraffin. Paraffin blocks were sectioned with a sliding microtome at the thickness of 4 µm. Tissue sections were deparaffinized and rehydrated. Heat-induced antigen retrieval was performed in Histofine® antigen retrieval solution (pH 9) (Nichirei, Tokyo, Japan) following manufacturer's protocol. Tissue sections

were blocked with 5% normal goat serum at room temperature for 1 h, then incubated in primary antibody solution at 4 °C overnight. After that, the sections were incubated in biotin-conjugated goat anti-rabbit IgG for 45 min, following by VECTASTAIN Elite ABC-HRP reagents per company's protocol, and finally stained with DAB and hematoxylin nuclear counterstaining. Tissue sections were mounted using PathoMount (Wako, Japan), and observed under Keyence BZ-X800 Fluorescent Microscope (RRID:SCR_023617).

CellROX staining

CT and KO B16F10 cells were cultured in DMEM with 10% FBS overnight. The cells were separated in three groups (n = 3 per group), 10% FBS, 1% FBS, and tert-Butyl hydroperoxide (TBHP) group. 10%FBS and THBP groups were cultured in DMEM with 10% FBS for 24 h, while 1%FBS group was cultured in DMEM with 1% FBS for 24 h, prior to staining. We used CellROX™ Green Flow Cytometry Assay Kit according to manufacturer's protocol, to measure oxidative stress capacity. Briefly, the TBHP group was added with 200 μM TBHP for 30 min prior to staining. The cells were then stained with 500 μM CellROX solution for 30 min. 2500 μM n-Acetylcysteine was used as negative control. After staining, the cells were collected and analyzed for green fluorescence by flow cytometry and recorded as mean fluorescence intensity (MFI).

Lipidomics analysis

Cells were cultured in DMEM with 10% FBS for 24 h, before collected by trypsinization and stored in PBS at -80 °C until analysis. Lipidomics analysis was performed by Human Metabolome Technologies, Inc., using liquid chromatography-mass spectrophotometry (LC–MS/MS) technique.

Statistical analysis

All data represent the mean ± s.d., calculated from at least three independent experiments. Statistical comparisons were analyzed using Student's unpaired t-test (two-tailed), multiple t-test with FDR correction, or two-way ANOVA test. Statistical significances were considered at p-value < 0.05. The analyses were performed using GraphPad Prism v10.0.2 (http://www.graphpad.com/ , RRID:SCR_002798), and Microsoft Excel v16.78 (https://www.microsoft.com/en-gb/, RRID:SCR_016137).

Data availability

The additional datasets generated during and/or analyzed during the current study, that are not included in this published article, are available from the corresponding author on reasonable request.

Received: 19 July 2024; Accepted: 22 November 2024
Published online: 26 March 2025

References

1. Long, G. V., Swetter, S. M., Menzies, A. M., Gershenwald, J. E. & Scolyer, R. A. Cutaneous melanoma. *The Lancet* **402**, 485–502 (2023).
2. Diener, J. & Sommer, L. Reemergence of neural crest stem cell-like states in melanoma during disease progression and treatment. *Stem Cells Transl Med* **10**, 522–533 (2021).
3. Kim, I. S. et al. Microenvironment-derived factors driving metastatic plasticity in melanoma. *Nat Commun* **8**, 14343 (2017).
4. Diazzi, S., Tartare-Deckert, S. & Deckert, M. The mechanical phenotypic plasticity of melanoma cell: an emerging driver of therapy cross-resistance. *Oncogenesis* **12**, 7 (2023).
5. Pedri, D., Karras, P., Landeloos, E., Marine, J.-C. & Rambow, F. Epithelial-to-mesenchymal-like transition events in melanoma. *FEBS J* **289**, 1352–1368 (2022).
6. Hoek, K. S. et al. In vivo switching of human melanoma cells between proliferative and invasive states. *Cancer Res* **68**, 650–656 (2008).
7. Verfaillie, A. *et al.* Decoding the regulatory landscape of melanoma reveals TEADS as regulators of the invasive cell state. *Nat Commun* **6** (2015).
8. Arozarena, I. & Wellbrock, C. Phenotype plasticity as enabler of melanoma progression and therapy resistance. *Nat Rev Cancer* **19**, 377–391 (2019).
9. Tirosh, I. et al. Dissecting the multicellular ecosystem of metastatic melanoma by single-cell RNA-seq. *Science* **1979**(352), 189–196 (2016).
10. Wellbrock, C. & Arozarena, I. Microphthalmia-associated transcription factor in melanoma development and MAP-kinase pathway targeted therapy. *Pigment Cell Melanoma Res* **28**, 390–406 (2015).
11. Kawakami, A. & Fisher, D. E. The master role of microphthalmia-associated transcription factor in melanocyte and melanoma biology. *Laboratory Investigation* **97**, 649–656 (2017).
12. Nyakas, M. et al. AXL inhibition improves BRAF-targeted treatment in melanoma. *Sci Rep* **12**, 5076 (2022).
13. Martínez-Reyes, I. & Chandel, N. S. Cancer metabolism: Looking forward. *Nature Reviews Cancer* **21**, 669–680 (2021).
14. Martinez-Outschoorn, U. E., Peiris-Pagés, M., Pestell, R. G., Sotgia, F. & Lisanti, M. P. Cancer metabolism: A therapeutic perspective. *Nature Reviews Clinical Oncology* **14**, 11–31 (2016).
15. Cantley, L. C. The phosphoinositide 3-kinase pathway. *Science* **1979**(296), 1655–1657 (2002).
16. Tímár, J., Hegedüs, B. & Rásó, E. The role of lipid signaling in the progression of malignant melanoma. *Cancer and Metastasis Reviews* **37**, 245–255 (2018).
17. Pascual, G. et al. Targeting metastasis-initiating cells through the fatty acid receptor CD36. *Nature* **541**, 41–45 (2017).
18. Rambow, F. et al. Toward minimal residual disease-directed therapy in melanoma. *Cell* **174**, 843-855.e19 (2018).
19. Ubellacker, J. M. et al. Lymph protects metastasizing melanoma cells from ferroptosis. *Nature* **585**, 113–118 (2020).
20. Vivas-García, Y. et al. Lineage-restricted regulation of SCD and fatty acid saturation by MITF controls melanoma phenotypic plasticity. *Mol Cell* **77**, 120-137.e9 (2020).
21. Du, J. *et al.* Raman-guided subcellular pharmaco-metabolomics for metastatic melanoma cells. *Nat Commun* **11** (2020).
22. Maximin, E. et al. Fatty acid binding protein 7 and n-3 poly unsaturated fatty acid supply in early rat brain development. *Dev Neurobiol* **76**, 287–297 (2016).
23. Balendiran, G. K. et al. Crystal structure and thermodynamic analysis of human brain fatty acid-binding protein. *Journal of Biological Chemistry* **275**, 27045–27054 (2000).

24. Foerster, S. et al. The fatty acid binding protein FABP7 is required for optimal oligodendrocyte differentiation during myelination but not during remyelination. *Glia* **68**, 1410–1420 (2020).
25. Hamilton, H. L. et al. FABP7 drives an inflammatory response in human astrocytes and is upregulated in Alzheimer's disease. *Geroscience* **46**, 1607–1625 (2024).
26. Tripathi, S. et al. Docosahexaenoic acid up-regulates both PI3K/AKT-dependent FABP7–PPARγ interaction and MKP3 that enhance GFAP in developing rat brain astrocytes. *J Neurochem* **140**, 96–113 (2017).
27. Wolfrum, C. Cytoplasmic fatty acid binding protein sensing fatty acids for peroxisome proliferator activated receptor activation. *Cellular and Molecular Life Sciences* **64**, 2465–2476 (2007).
28. Kagawa, Y. et al. Role of FABP7 in tumor cell signaling. *Adv Biol Regul* **71**, 206–218 (2019).
29. Umaru, B. A. et al. Oleic acid-bound FABP7 drives glioma cell proliferation through regulation of nuclear lipid droplet formation. *FEBS J* **290**, 1798–1821 (2023).
30. Kagawa, Y. et al. Nuclear FABP7 regulates cell proliferation of wild-type IDH1 glioma through caveolae formation. *Mol Oncol* **16**, 289–306 (2022).
31. Nagao, K. *et al.* Fatty acid binding protein 7 may be a marker and therapeutic targets in clear cell renal cell carcinoma. *BMC Cancer* **18** (2018).
32. Bensaad, K. et al. Fatty Acid uptake and lipid storage induced by HIF-1α contribute to cell growth and survival after hypoxia-reoxygenation. *Cell Rep* **9**, 349–365 (2014).
33. Umaru, B. A. et al. Ligand bound fatty acid binding protein 7 (FABP7) drives melanoma cell proliferation via modulation of Wnt/β-catenin signaling. *Pharm Res* **38**, 479–490 (2021).
34. Goto, Y. et al. Aberrant fatty acid-binding protein-7 gene expression in cutaneous malignant melanoma. *Journal of Investigative Dermatology* **130**, 221–229 (2010).
35. Slipicevic, A. et al. The fatty acid binding protein 7 (FABP7) is involved in proliferation and invasion of melanoma cells. *BMC Cancer* **8**, 1–13 (2008).
36. Goto, Y. et al. A new melanoma antigen fatty acid-binding protein 7, involved in proliferation and invasion, is a potential target for immunotherapy and molecular target therapy. *Cancer Res* **66**, 4443–4449 (2006).
37. Seliger, B., Wollscheid, U., Momburg, F., Blankenstein, T. & Huber, C. Characterization of the major histocompatibility complex class I deficiencies in B16 melanoma cells1. *Cancer Res* **61**, 1095–1099 (2001).
38. Xu, J., Lamouille, S. & Derynck, R. TGF-β-induced epithelial to mesenchymal transition. *Cell Research* **19**, 156–172 (2009).
39. Fidler, I. J. Selection of successive tumour lines for metastasis. *Nature New Biology* **242**, 148–149 (1973).
40. Hill, R. P., Chambers, A. F., Ling, V. & Harris, J. F. Dynamic heterogeneity: Rapid generation of metastatic variants in mouse B16 melanoma cells. *Science* **1979**(224), 998–1001 (1984).
41. Zadoorian, A., Du, X. & Yang, H. Lipid droplet biogenesis and functions in health and disease. *Nature Reviews Endocrinology* **19**, 443–459 (2023).
42. Vaziri-Gohar, A. *et al.* Limited nutrient availability in the tumor microenvironment renders pancreatic tumors sensitive to allosteric IDH1 inhibitors. *Nature Cancer* **3**, 852–865 (2022).
43. Munir, R., Lisec, J., Swinnen, J. V. & Zaidi, N. Lipid metabolism in cancer cells under metabolic stress. *Br J Cancer* **120**, 1090–1098 (2019).
44. Quail, D. F. & Joyce, J. A. Microenvironmental regulation of tumor progression and metastasis. *Nature Medicine* **19**, 1423–1437 (2013).
45. Avagliano, A. *et al.* Metabolic Plasticity of melanoma cells and their crosstalk with tumor microenvironment. *Front Oncol* **10** (2020).
46. Marzagalli, M., Ebelt, N. D. & Manuel, E. R. Unraveling the crosstalk between melanoma and immune cells in the tumor microenvironment. *Semin Cancer Biol* **59**, 236–250 (2019).
47. Currie, E., Schulze, A., Zechner, R., Walther, T. C. & Farese, R. V. Cellular fatty acid metabolism and cancer. *Cell Metab* **18**, 153–161 (2013).
48. Falletta, P. et al. Translation reprogramming is an evolutionarily conserved driver of phenotypic plasticity and therapeutic resistance in melanoma. *Genes Dev* **31**, 18–33 (2017).
49. Wang, D. & Dubois, R. N. Eicosanoids and cancer. *Nature Reviews Cancer* **10**, 181–193 (2010).
50. Kagawa, Y. et al. Fatty acid-binding protein 7 regulates function of caveolae in astrocytes through expression of caveolin-1. *Glia* **63**, 780–794 (2015).
51. Razani, B. et al. Caveolin-1 Regulates Transforming Growth Factor (TGF)-β/SMAD Signaling through an Interaction with the TGF-β Type I Receptor. *Journal of Biological Chemistry* **276**, 6727–6738 (2001).
52. Cano, A. *et al.* The transcription factor Snail controls epithelial–mesenchymal transitions by repressing E-cadherin expression. *Nature Cell Biology* **2**, 76–83 (2000).
53. Yang, H. et al. TGF-β-activated SMAD3/4 complex transcriptionally upregulates N-cadherin expression in non-small cell lung cancer. *Lung Cancer* **87**, 249–257 (2015).
54. Yuan, S., Norgard, R. J. & Stanger, B. Z. Cellular plasticity in cancer. *Cancer Discov* **9**, 837–851 (2019).
55. Park, S. M., Gaur, A. B., Lengyel, E. & Peter, M. E. The miR-200 family determines the epithelial phenotype of cancer cells by targeting the E-cadherin repressors ZEB1 and ZEB2. *Genes Dev* **22**, 894–907 (2008).
56. Iqbal, M. J. et al. Interplay of oxidative stress, cellular communication and signaling pathways in cancer. *Cell Communication and Signaling* **22**, 1–16 (2024).
57. Islam, A. et al. FABP7 protects astrocytes against ROS toxicity via lipid droplet formation. *Mol Neurobiol* **56**, 5763–5779 (2019).
58. Abdelwahab, S. A. et al. Localization of brain-type fatty acid-binding protein in Kupffer cells of mice and its transient decrease in response to lipopolysaccharide. *Histochem Cell Biol* **119**, 469–475 (2003).
59. Kagawa, Y. et al. Mitochondrial dysfunction in GnRH neurons impaired GnRH production. *Biochem Biophys Res Commun* **530**, 329–335 (2020).

Acknowledgements

We would like to thank the Biomedical Research Core, Graduate School of Medicine, Tohoku university, Japan, for their equipment support. This project was funded by JSPS KAKENHI Grant Numbers 22K19724 and 22H03526 (to YO).

Author contributions

T.W., H.M., and Y.O. contributed to conceptualization and experimental plans. T.W. and H.M. performed the experiments. T.W. analyzed the data. T.W. and H.M. wrote the manuscript. All others contributed to reviewing and editing the manuscript; Y.O. contributed to supervising and funding.

Declarations

Competing interests
The authors declare no competing interests.

Additional information
Supplementary Information The online version contains supplementary material available at https://doi.org/10.1038/s41598-024-80874-5.

Correspondence and requests for materials should be addressed to H.M.

Reprints and permissions information is available at www.nature.com/reprints.

Publisher's note Springer Nature remains neutral with regard to jurisdictional claims in published maps and institutional affiliations.